

Nodal Semimetals: A Survey on Optical Conductivity

Artem V. Pronin* and Martin Dressel

Among different topological and related phases of condensed matter, nodal semimetals occupy a special place—the electronic band topology in these materials is related to 3D bulk, rather than to surface, states. A great variety of different realizations of electronic band crossings (the nodes) leads to a plethora of different electronic properties, ranging from chiral anomaly to solid-state realizations of a black-hole horizon. The different nodal phases have similar low-energy band structure and quasiparticle dynamics, which both can be accessed experimentally by a number of methods. Optical measurements with their large penetration depth and high energy resolution are ideally suited as such a bulk probe, especially at low energies where other spectroscopic methods often lack the required resolution. Herein, recent optical conductivity studies of different nodal semimetals are reviewed, possible limitations of such measurements are discussed, and a comparison between the experimental results, simple theoretical models, and band-structure-based calculations is provided.

1. Introduction

Succeeding graphene and topological insulators, nodal semimetals came into focus of condensed matter physics a few years ago.^[1–24] In these 3D materials, linearly dispersing electronic bands possess point and/or line crossings in the vicinity of the chemical potential in the bulk Brillouin zone (BZ). These bulk band crossings may lead to topologically trivial (as in the case of Dirac semimetals) or nontrivial (e.g., in Weyl semimetals) electronic phases. Important is that the low-energy electronic dispersion relations can be approximated by a solution of Dirac equation or its modifications.^[25] This makes the optical (interband) response of nodal semimetals generally different from the response of “ordinary” 3D metals and semiconductors and often allows probing the low-energy band structure via optical conductivity measurements. The studies on nodal semimetals, where the linear frequency-dependent conductivity, $\sigma(\omega) = \sigma_1(\omega) + i\sigma_2(\omega)$, was measured, were the focus of many recent experimental reports. Such measurements reflect the bulk

material properties, as the skin depth is typically above a few tens of nanometers for any measurement frequency and of the order of 100 nm–1 μ m for the most interesting far-infrared portion of the spectrum.^[26–28] In this article, we summarize our findings obtained in such measurements within the past few years and review the most relevant optical results from literature.

In the discussion, we concentrate exclusively on the optical conductivity features related to the electronic band structure. In addition, optical spectra may contain information on such effects as strong electron–electron or electron–phonon coupling. Possible importance of these interactions in different Dirac materials is widely debated.^[29–35] It looks like the majority of experimental results on nodal semimetals

(particularly, for nonmagnetic systems) can be understood within a single-particle picture. Still, there are reports on the experimental detection of different collective effects, also by optical means. For example, a density-wave formation was suggested in the Dirac semimetal $\text{Ca}_{1-x}\text{Na}_x\text{MnBi}_2$ ^[36] and a strong coupling between optical phonons and Weyl quasiparticles was discussed in TaAs.^[37] Reviewing such effects is not the scope of this article. Herein, we just note that in all examples discussed later the collective effects do not manifest themselves in optical conductivity in an explicit way. For instance, the phonon modes remain sharp (and of Lorentzian shape), even though these modes overlap in frequency with the interband (Drude) response of conducting carriers, e.g., refer the studies by Neubauer et al. and Maulana et al.^[27,38]

2. Theoretical Background: Electronic Band Dispersion and Optical Conductivity


In this section, we briefly recap theoretical predictions for the frequency behavior of optical conductivity in the major types of nodal semimetals (see **Figure 1** for schematic diagrams of their band structures). More details for specific cases can be found in vast available literature, especially in the works of Carbotte and coworkers.^[39–48]

In the case of electron–hole symmetric d -dimensional bands with $E(\mathbf{k}) \propto |\mathbf{k}|^z$, the real part of the interband optical conductivity is supposed to follow a power–law frequency dependence^[49,50]

$$\sigma_1^{\text{IB}}(\omega) \propto \omega^{(d-2)/z} \quad (1)$$

For Dirac and Weyl semimetals, $d = 3$, the bands are conical ($z = 1$), and Equation (1) can be more specifically rewritten as

Dr. A. V. Pronin, Prof. M. Dressel
1. Physikalisches Institut
Universität Stuttgart
Pfaffenwaldring 57, 70569 Stuttgart, Germany
E-mail: artem.pronin@pi1.physik.uni-stuttgart.de

 The ORCID identification number(s) for the author(s) of this article can be found under <https://doi.org/10.1002/pssb.202000027>.

© 2020 The Authors. Published by WILEY-VCH Verlag GmbH & Co. KGaA, Weinheim. This is an open access article under the terms of the Creative Commons Attribution License, which permits use, distribution and reproduction in any medium, provided the original work is properly cited.

DOI: 10.1002/pssb.202000027

$$\sigma_1^{\text{IB}}(\omega) = \frac{e^2 N_{\text{W}} \omega}{12h v_{\text{F}}} \quad (2)$$

where N_{W} is the number of Weyl nodes (for a single Dirac node, $N_{\text{W}} = 2$), v_{F} is the Fermi velocity, $h = 2\pi\hbar$ is the Planck constant, and all Weyl/Dirac bands are considered to be identical (up to a spin degree of freedom) with their nodes situated at the chemical potential μ . If the node position is not at the chemical potential ($\mu \neq 0$), transitions for the energies below 2μ are Pauli blocked, and Equation (2) is modified to

$$\sigma_1^{\text{IB}}(\omega) = \frac{e^2 N_{\text{W}} \omega}{12h v_{\text{F}}} \theta\{\hbar\omega - 2\mu\} \quad (3)$$

where $\theta\{x\}$ is the Heaviside step function and any carrier scattering is ignored. In this case, an intraband contribution to conductivity will also be present in the spectra. For finite electron scattering, the Heaviside function can be replaced, for example, by

$$\frac{1}{2} + \frac{1}{\pi} \arctan \frac{\omega - 2\mu/\hbar}{\gamma} \quad (4)$$

with γ representing an appropriate scattering rate, and intraband conductivity can be approximated by a standard Drude ansatz.^[51]

In the study by Carbotte,^[40] it was shown that tilting the conical bands (relevant, e.g., for type-II Weyl semimetals^[52,53]) affects the linear behavior of optical conductivity: $\sigma_1^{\text{IB}}(\omega)$ remains (quasi) linear but experiences slope changes at certain frequency points, whose positions are related to μ and the tilt angle.

For generalizations of Weyl bands with higher Chern numbers,^[7,23,54–57] the shape of $\sigma_1^{\text{IB}}(\omega)$ depends on the band dispersion relations. In the so-called multifold semimetals, where a few linear (rotationally symmetric) bands with generally different slopes cross at a given point of the BZ,^[7,23] the optical conductivity is linear in frequency (up to the steps, related to the Pauli-blocked transitions).^[58] For more complicated band structures, such as touching bands with a linear dispersion in one direction and parabolic dispersions in the remaining two,^[54,55] $\sigma_1^{\text{IB}}(\omega)$ is expected to be anisotropic,^[59] in accordance with Equation (1). In addition, if the nodes are situated at different energies, as appearing, e.g., in real multifold semimetals, $\sigma_1^{\text{IB}}(\omega)$ changes its frequency run at different energy scales. The important point is that the total interband $\sigma_1(\omega)$ can often be decomposed into contributions from the nodes of each kind, simplifying interpretation of experimental spectra.

A particularly interesting case is the nodal-line semimetals (NLSMs),^[5] where the presence of a continuous line of nodes effectively reduces the dimensionality of the crossing electronic bands to $d = 2$. This reduced dimensionality leads to a frequency-independent $\sigma_1^{\text{IB}}(\omega)$ according to Equation (1). Earlier, such “flat” optical conductivities were predicted and experimentally observed in graphene and graphite^[60–62] with a universal conductance value per one graphene sheet, $\pi e^2 / (2h)$. In NLSMs, no universal sheet conductance is expected; instead, $\sigma_1^{\text{IB}}(\omega)$ is related to the length of the nodal line k_0 in a BZ.^[43,44,63] For a circular nodal line, one has



Artem V. Pronin received his PhD degree from the Moscow Institute of Physics and Technology, Russia, in 1998. He has held postdoctoral positions at McMaster University, Canada, and Leiden University, the Netherlands. Later, he joined the Hochfeld-Magnetlabor Dresden, Germany, where he carried out infrared and THz measurements in high magnetic fields. Since 2015, he has been leading a group at the 1. Physikalisches Institut, Universität Stuttgart, Germany. The group investigates optical properties of different topological materials.



Martin Dressel received his PhD degree from the Universität Göttingen, Germany, in 1989. Since then, he has held positions at the Laser Laboratory Göttingen, the University of British Columbia, Canada, and the University of California, Los Angeles, USA. He received his Habilitation from the Technische Universität Darmstadt, Germany, in 1996, and then joined the Center for Electronic Correlations and Magnetism, Universität Augsburg, Germany. Since 1998, he has been Head of the 1. Physikalisches Institut, Universität Stuttgart, Germany. His laboratory is one of the leading places for microwave, THz, and infrared spectroscopy of solids.

$$\sigma_1^{\text{IB}}(\omega) = \frac{e^2 k_0}{16h} \quad (5)$$

It is assumed here that the plane of the nodal circle is perpendicular to the electric-field component of the probing radiation and that there is no particle–hole asymmetry. For $\mu \neq 0$, a Pauli edge (Equation (3) and (4)) occurs in the conductivity spectra.

3. Linear Optical Response: Review of Experimental Results

3.1. Experiments Versus Computations

A large number of recent experiments are devoted to measuring optical conductivity in nodal-semimetal candidates.^[26–28,36,38,64–77] There are also theoretical studies, where $\sigma(\omega)$ is computed for particular semimetal compounds based on their band-structures.^[78–82] Some studies combine both, experiment and band-structure-based computations.^[27,28,83–85] We would like to stress here that usually the match between measurements and such computations is only qualitative. **Figure 2** and **3** show two typical examples of the theory-versus-experiment spectra comparison—for YbMnBi₂ and NbP, correspondingly. In both cases, the calculations reproduce the major features observed in the experimental conductivity but fail to catch the exact frequency positions of the features and their spectral shapes. This result is not surprising, considering the well-known

difficulties of ab initio optical conductivity calculations, especially at low frequencies. It seems optimal to combine experimental studies with simple-model (or effective-Hamiltonian) approaches as well as ab initio calculations, as attempted, e.g., in the studies by Maulana et al., Chaudhuri et al., Ebad-Allah et al., Shao et al.^[38,83–85] This may allow a deeper insight into the relation between the semimetal band structure and its optical conductivity. In addition, band-selective optical-conductivity calculations are quite helpful. Such calculations are, however, rarely carried out.^[27,83,84]

3.2. Nodal-Line Semimetals

3.2.1. ZrSiS and Its Relatives

We start reviewing optical conductivity measurements of nodal semimetals with ZrSiS. The reason for this is a relatively

simple, basically model, band structure of this layered, quasi-2D, compound. (We note that all currently available optical measurements of ZrSiS and its relatives were carried out on in-plane surfaces and showed no anisotropy, consistent with the tetragonal in-plane symmetry of these compounds.) ZrSiS possesses a nodal line, situated near the Fermi level.^[86,87] Although the shape of the line is rather complex and, furthermore, the line is slightly gapped due to spin-orbit coupling (SOC), the linearity of the electronic bands forming this nodal line extends up to ≈ 0.5 eV, and other (nonlinear) bands do not cross the Fermi level. This makes ZrSiS one of the best systems for searching the signatures of Dirac electrons in the optical conductivity spectra.

Measurements of the optical conductivity in ZrSiS have been reported in previous studies.^[26,84,88,89] **Figure 4** shows the real part of the optical conductivity obtained in the study by Schilling et al.^[26] The striking feature of the spectra is the flat,

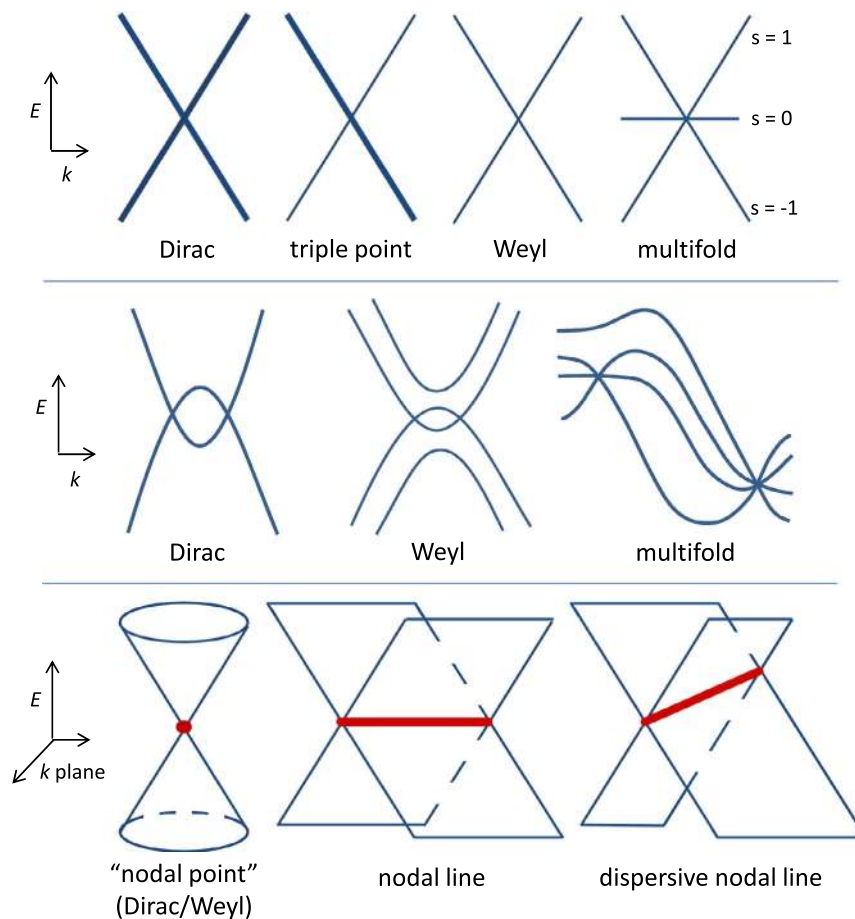


Figure 1. Model band structures for different nodal semimetals. Upper row: schematic band dispersions near the nodes in Dirac, triple-point, Weyl, and multifold semimetals (from left to right). The multifold semimetal dispersion is presented for a spin 1 threefold fermion case. Middle row: more realistic (but still schematic) band structures, related to the compounds considered in this Review—Dirac (Cd_3As_2), Weyl (the TaAs family), and multifold semimetals (RhSi and other materials from the space group no. 198). For the latter case, the electronic bands are shown without SOC being included (cf. the accurate band structure calculations for RhSi in Figure 12). For a triple-point realistic band dispersion, refer to Figure 10. In the two upper rows, the band degeneracy is encoded as the line thickness—thin lines represent nondegenerate bands, whereas thick lines represent (doubly) degenerate bands. Bottom row: a graphical explanation of the differences between the Dirac (or Weyl) semimetals (left picture) and NLSMs (middle and right pictures). The band crossings are depicted as bold red points and lines. Note that the actual k -space is 3D; thus, the shown figures are the relevant cuts of the full (4D) $E(k)$ pictures.

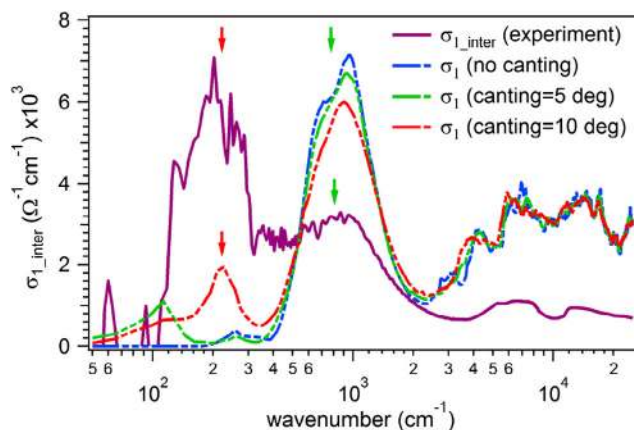


Figure 2. Optical conductivity of YbMnBi₂. The solid magenta line shows experimental interband conductivity (i.e., the Drude contribution is subtracted) at 5 K. The other curves are band-structure-based calculations for different canting angles of Mn²⁺ magnetic moments. Reproduced with permission.^[83] Copyright 2017, American Physical Society.

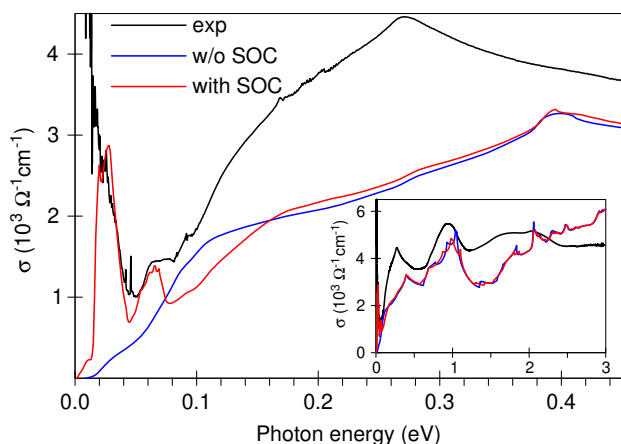


Figure 3. Interband optical conductivity of NbP calculated from its band structure with (red line) and without (blue line) SOC and the total (i.e., inter- and intraband) experimental NbP conductivity at 10 K (black line). Intraband (Drude) contributions to the conductivity are not included in the computations. Inset shows same sets of data on a broader frequency scale. All spectra are for the (001)-plane response. Reproduced with permission.^[27] Copyright 2018, American Physical Society.

frequency-independent, region, spanning from 250 to 2500 cm⁻¹ (30–300 meV) for almost all temperatures investigated (at $T \geq 100$ K, the flat region starts at a bit higher frequencies because of a broadened free-electron Drude mode). This observation is in perfect agreement with the simple-model predictions for NLSMs discussed above (Equation (1) and (5)).

The sharp dip in the 10 K spectra could be interpreted as either a Pauli edge or the spin-orbit gap, enabling hence the upper estimate for the gap of ≈ 30 meV. Our later magneto-optical investigations provide a more accurate value of 26 meV,^[89] in a reasonable agreement with the calculated value of 15 meV.^[86]

As the frequency increases toward higher than 400 meV, $\sigma_1(\omega)$ first decreases and then increases again, demonstrating a U-shape

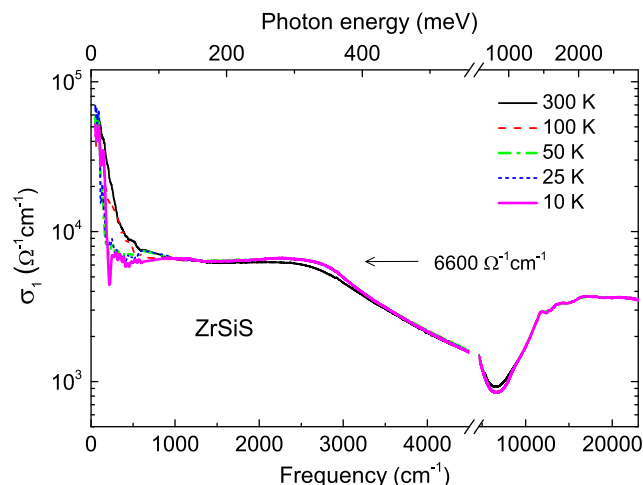


Figure 4. In-plane optical conductivity of ZrSiS. Reproduced with permission.^[26] Copyright 2017, American Physical Society.

behavior. Similar behavior was also observed in a number of related compounds—ZrSiSe, ZrGeS, and ZrGeTe^[84]—and reproduced in band-structure-based calculations for all four materials.^[80,84] Interpretation of the high-energy upturn of the U-shaped conductivity is rather straightforward—it is due to transitions between almost-parallel bands near the X and R points of the BZ of these compounds.

According to the study by Ebad-Allah et al.,^[84] the low-energy part of the U-shaped conductivity, where $\sigma_1(\omega)$ is roughly proportional to $1/\omega$, can be interpreted as being due to a “nodal plane” (Equation (1) for Dirac bands and $d = 1$). In other words, there is a further electronic-band dimensionality reduction due to the quasi-2D (band) structure of these compounds: the dispersion is linear only in one \mathbf{k} -space direction, whereas it is almost absent along the nodal line, as well as in the out-of-plane direction. This nodal-plane picture can only work for relatively high frequencies, as otherwise the band structure cannot be approximated as 2D. Indeed, a basically frequency-independent $\sigma_1^{\text{IB}}(\omega)$ is observed at low frequencies (below 0.4–0.5 eV) in all four materials, albeit the frequency span of the flat conductivity is largest in ZrSiS.

These flat areas of $\sigma_1^{\text{IB}}(\omega)$ cannot be accurately reproduced by the available calculations based on the band structure.^[80,84] Instead, the calculated low-energy $\sigma_1^{\text{IB}}(\omega)$ is found to increase with frequency. Habe and Koshino^[80] suggested that the observed flat conductivity might be a cumulative effect of the increasing interband conductivity and a decreasing Drude contribution. However, the experimental data do not support this explanation. As shown in Figure 4, the Drude term is very narrow and does not overlap with the flat region. Also, it is the interband conductivity (i.e., the conductivity after subtraction of the Drude modes), which shows the almost flat regions at low energies in the study by Ebad-Allah et al.^[84]

Overall, the flat interband conductivity of ZrSiS at low energies is a robust experimental result (in ZrSiSe, ZrGeS, and ZrGeTe, similar behavior is observed). The simple interpretation based on Equation (1) and (5) offers a good qualitative interpretation of this result. More advanced band-structure-based

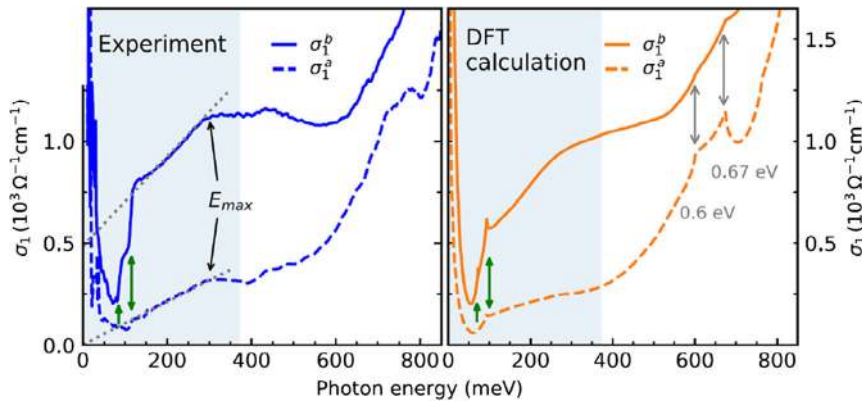


Figure 5. Optical conductivity of NbAs₂ for two different crystallographic directions. Left panel—experiment and right panel—DFT calculations. Reproduced with permission.^[85] Copyright 2019, The Authors, published by PNAS.

calculations of optical conductivity are required to provide a full description for these observations.

3.2.2. NbAs₂

This material is another example of NLSM. Unlike ZrSiS, the nodal lines in NbAs₂ do not form closed loops or cages in a BZ but span from one BZ to another. Most importantly, the nodal lines in NbAs₂ are “dispersive,” meaning that the nodal-line energy position depends on the momentum. In fact, the nodal lines in ZrSiS and its relatives also possess such dispersion. However, it is much weaker than in NbAs₂ and does not seem to affect the optical spectra appreciably. Similarly to ZrSiS, the nodal lines in NbAs₂ are gapped. Shao et al.^[85] found in NbAs₂ experimentally and also showed analytically that the optical conductivity due to the transitions between the linear bands, crossing along such dispersive nodal lines, demonstrates a linear-in-frequency, rather than a frequency-independent, behavior.

Indeed, the slope of the nodal line (i.e., $\partial E/\partial k_{\parallel}$, where k_{\parallel} represents the k direction along the nodal line) plays the same role as the Fermi velocity of a linear band. Thus, for a band with a relatively large $\partial E/\partial k_{\parallel}$, there will be no dimensionality reduction and the band can be considered as a 3D Dirac band with anisotropic Fermi velocity. If $v_{\parallel} = \partial E/\partial k_{\parallel}$ is not negligible, but still much smaller than the Fermi velocities in the directions perpendicular to the nodal line, v_{\perp} will mostly be responsible for the slope of $\sigma_1^{\text{IB}}(\omega)$. The linear increase in $\sigma_1^{\text{IB}}(\omega)$ is limited in frequency by the energy, corresponding to the difference between the extrema of the nodal-line energy positions. Above this frequency, $\sigma_1^{\text{IB}}(\omega)$ becomes frequency independent (if the bands forming the nodal line retain their linearities at these energies).

Such behavior of optical conductivity was recorded in NbAs₂, see **Figure 5**. The optical conductivity is anisotropic, because the nodal lines span almost parallel to the a axis. The linear behavior of $\sigma_1^{\text{IB}}(\omega)$ is clearly seen in the measurements and can be nicely reproduced by density functional theory (DFT) calculations. Perhaps, it is the best match between experiment and ab initio calculations reported for a nodal semimetal so far.

3.3. Weyl and Dirac Semimetals

3.3.1. TaAs Family

TaAs was one of the first confirmed Weyl semimetals,^[14,15,90] and its optical conductivity was reported as early as in 2016.^[68] This compound, as well as its family members (TaP, NbAs, and NbP), possesses 24 Weyl nodes, i.e., 12 pairs of the nodes with opposite chiralities.^[14,15,17,91] The nodes are “leftovers” of nodal rings, which are gapped by SOC everywhere in the BZ, except at these special points. The nodes can be divided in two groups, commonly dubbed as W1 ($N_{\text{W1}} = 8$) and W2 ($N_{\text{W2}} = 16$). According to band-structure calculations, in TaAs, the W1 (W2) nodes are situated at around 20–25 meV (10 meV) below the Fermi level.^[79,91]

Figure 6 shows the real part of TaAs optical conductivity obtained in the study by Xu et al.^[68] The zero-frequency-centered Drude mode is followed by an almost linear $\sigma_1(\omega)$, which

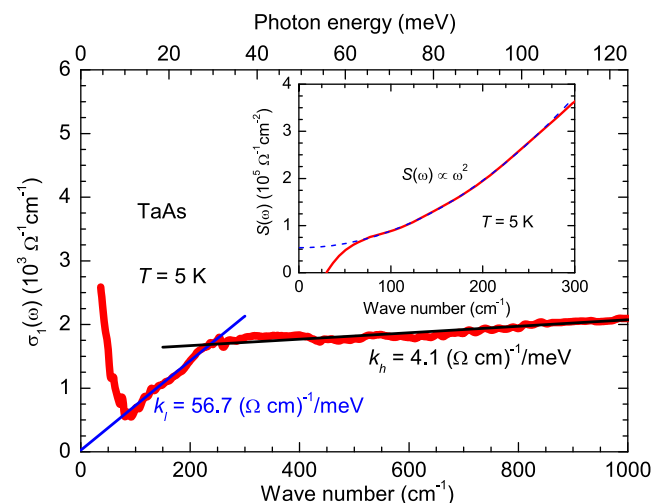


Figure 6. Optical conductivity of TaAs. The inset shows the optical spectral weight, $S(\Omega) = \int_0^{\Omega} \sigma_1(\omega) d\omega$. The quadratic $S(\Omega)$ corresponds to $\sigma_1 \propto \omega$. Reproduced with permission.^[68] Copyright 2016, American Physical Society.

changes its slope at around 25 meV. The low-frequency linear $\sigma_1(\omega)$ can be associated with the transitions between the linearly dispersing bands near the low-energy (W2) nodes. According to the spectra, the Pauli edge for these transitions should be situated at or below 10 meV, implying that the nodes are 5 meV off the Fermi level. This is not in disagreement with the band-structure calculations mentioned earlier: the accuracy of such calculations and the exact position of the Fermi level in a given sample are both within plus/minus a few meV.

The decreased slope of the linear $\sigma_1(\omega)$ for $\hbar\omega > 25$ meV may look puzzling at first glance: at higher energies, the W1 nodes should start contributing to $\sigma_1(\omega)$; hence, it should increase more rapidly with ω . To qualitatively explain the decreasing slope, one should recall that the Weyl nodes in TaAs are leftovers of gapped nodal lines. The bands, forming the W2 nodes, flatten out in the \mathbf{k} direction along the nodal lines at quite small energies (the nodal-line gap is in the tens-of-meV range). Thus, at these energies, the optical response starts to remind the nodal-line situation: $\sigma_1(\omega)$ is flattened.

One can notice that there is a small bump on the initial linear $\sigma_1(\omega)$ at around 15 meV. This bump was reproduced in later optical measurements of TaAs;^[92] a similar, but much stronger, peak was detected in TaP at comparable energies,^[92,93] see Figure 7. In the study by Kimura et al.^[92] these features were attributed to the transitions between the Lifshitz points of the bands forming the Weyl nodes (Figure 1, middle row).

Alternatively, such bumps might be related to the transitions between almost parallel bands split by SOC. Similar features were observed in our optical study of NbP at ≈ 30 and 60 meV (Figure 3) and interpreted as being due to such transitions, based on ab initio band-resolved optical conductivity calculations.^[27] We are not aware of any band-structure-based optical conductivity calculations for TaAs and TaP at low enough frequencies;

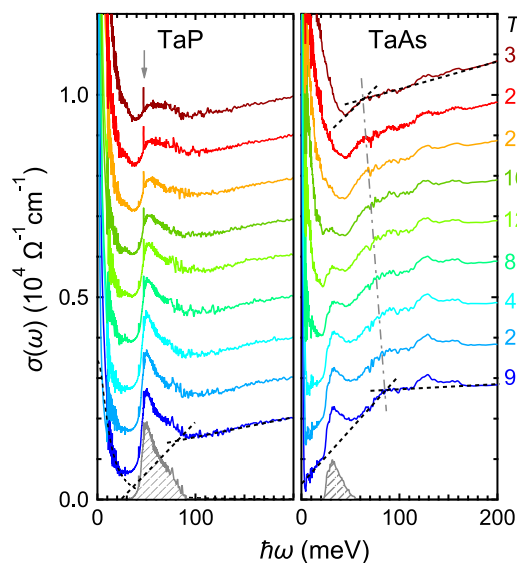


Figure 7. Optical conductivity of TaP and TaAs. The linear-in-frequency components of $\sigma_1(\omega)$ are best seen at lowest temperatures. The bumps at low energies might be similar to the bumps observed in NbP (cf. Figure 3 and 8). Reproduced with permission.^[92] Copyright 2017, American Physical Society.

thus, the correct interpretation of the observed low-energy peaks in these compounds is still to be found.

An interpretation of different spectral features detected in the optical conductivity of NbP is shown in Figure 8. The band-selective optical conductivity computations seem to be the best way for making such assignments.

All optical conductivity measurements of the TaAs family compounds discussed above have been carried out on (001) surfaces, which have tetragonal crystallographic symmetry and no optical anisotropy. The out-of-plane response (with the electric-field component of the probing light parallel to [001] direction) was studied by Levy et al.^[94] for TaAs. A linear increase in the low-energy interband conductivity was also observed for this polarization at the energies below 25 meV.

3.3.2. Cd_3As_2

Cadmium arsenide is one of the first discovered Dirac semimetals.^[9–12,95] Band structure calculations^[9] predict two Dirac cones per BZ in this material. Its optical conductivity was reported in a number of publications,^[70,96–99] and its (magneto)-optical properties were recently thoroughly reviewed.^[100]

In this brief Review, we would like to point out that the (almost) linear-in-frequency interband conductivity is observed in Cd_3As_2 up to very high frequencies, signaling a large energy scale of the (quasi)linear electronic bands, see Figure 9, where results collected on five different samples are shown. The Pauli edge is observed in the spectra at 600–1700 cm^{-1} , depending on the sample. This

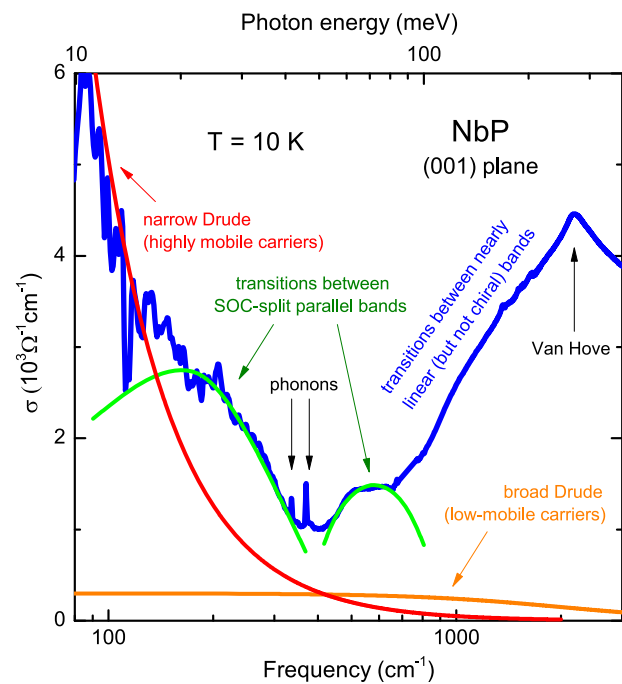


Figure 8. Optical conductivity of NbP and assignment of the observed features to different absorption mechanisms according to band-selective calculations. The conductivity contributions of these mechanisms are shown schematically as solid lines. Note logarithmic x-scale. Reproduced with permission.^[27] Copyright 2018, American Physical Society.

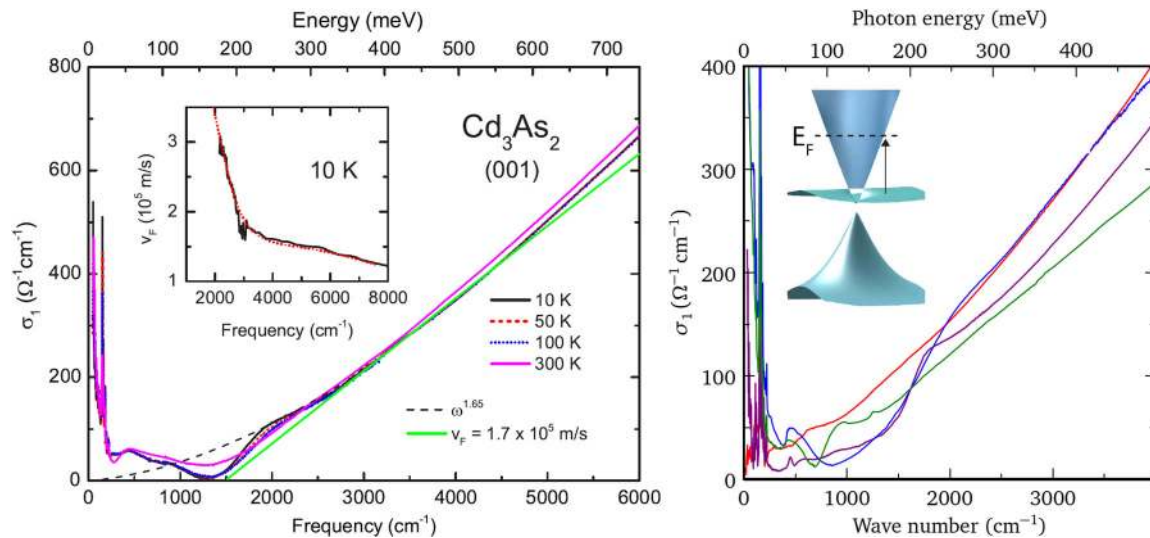


Figure 9. Optical conductivity of Cd_3As_2 studied on a few different samples. The left panel is adapted with permission.^[70] Copyright 2016, American Physical Society. The right panel is adapted with permission.^[96] Copyright 2018, American Physical Society. In the latter study, optical response from the (112) and (001) surfaces of different samples was collected, as shown by the red and purple curves (the (112)-surface response) and by the blue and green curves (the (001) response). The inset in the left panel demonstrates the k -averaged $\partial E/\partial k$, expressed as an energy-dependent Fermi velocity, for the (112)-plane measurements shown in this panel. Schematic of the Kane-model-like band structure, proposed for Cd_3As_2 as an alternative of Dirac cones, is depicted in the right panel.

large variation of the Pauli edge position is related to the naturally present As vacancies, whose concentration depends on sample-growth and annealing conditions. In addition, free carriers in Cd_3As_2 demonstrate nonuniform spatial distribution, forming charge puddles with characteristic scales of $100\ \mu\text{m}$, as demonstrated by optical microscopy.^[96]

A closer inspection of the conductivity spectra reveals a slight superlinear increase of $\sigma_1(\omega)$. This increase was attributed either to electron-self-energy effects or to deviations of the crossing bands from perfect linearity.^[70] In the latter case, $\partial E/\partial k$ is energy dependent, as shown in the inset of the left panel in Figure 9.

Concluding the subsection on Cd_3As_2 , we note that the picture with two Dirac bands extending up to high energies (hundreds of meV) has been challenged by magneto-optical measurements,^[98] which are best consistent with a Kane-like model^[101–103] with three electronic bands, one of the bands being almost flat. (Dirac cones may still appear in this model, but on a much smaller energy scale, see the diagram in the right panel of Figure 9.) The tunneling data^[95] can be (re)interpreted based on this model. It has been argued^[96] that $\sigma_1(\omega)$ spectra are also consistent with the model. Still, band-structure calculations and results of angle-resolved photoemission spectroscopy (ARPES) favor a Dirac, rather than a Kane-like, picture for Cd_3As_2 . A full consensus on the electronic band structure of this material is still to be established.

3.3.3. Semimetals with Strongly Tilted Dirac or Weyl Cones

As mentioned earlier, tilting the Dirac or Weyl cones should lead to the modifications of the interband optical conductivity: $\sigma_1^{\text{IB}}(\omega)$ is still linear but demonstrates changes in its slope at certain frequency points. A body of experimental work was conducted on materials with (supposedly) strongly tilted 3D Dirac or Weyl

cones.^[69,83,104–106] Linear portions of experimental $\sigma_1(\omega)$ were indeed reported, e.g., for YbMnBi_2 —a type-II Weyl semimetal candidate. However, intraband contribution often masks the interband optical transitions in such materials. This is particularly relevant for type-II semimetals, where free carriers exist even if the chemical potential is situated at the nodal point^[22] and, hence, Drude-like contributions are supposed to dominate the optical conductivity spectra. This was indeed observed, for example, in WTe_2 and MoTe_2 .^[105,106]

3.4. Triple-Point Semimetals

The existence of triple points, where one nondegenerate and one doubly degenerate bands cross, implies the presence of bulk nodal lines in the band structure of triple-point semimetals (TPSMs).^[22] Because of this band structure complexity, no simple models for the optical conductivity are available for these materials. Thus, a comparison between experiment and band-structure-based computations is the way to interpret $\sigma_1^{\text{IB}}(\omega)$ in TPSMs. As an example, we review here the results of our optical conductivity measurements in GdPtBi ,^[28] a TPSM and a member of the half-Heusler family, which is recognized for a broad variety of exotic and potentially functional properties.^[107,108]

In the paramagnetic state (GdPtBi enters the antiferromagnetic state at $9\ \text{K}$ ^[109]—this phase was not examined by optics), at low temperatures (e.g., at 10 – $50\ \text{K}$), we found $\sigma_1(\omega)$ in GdPtBi to be linear in a broad frequency range: the linearity spans down to $100\ \text{cm}^{-1}$, see **Figure 10a,d**, indicating a low free-carrier density. Unlike the situation in a simple conical band, this linearity is not due to the transitions within such a band. Our calculations showed instead that the linear $\sigma_1^{\text{IB}}(\omega)$ is a cumulative effect of transitions between a few bands with

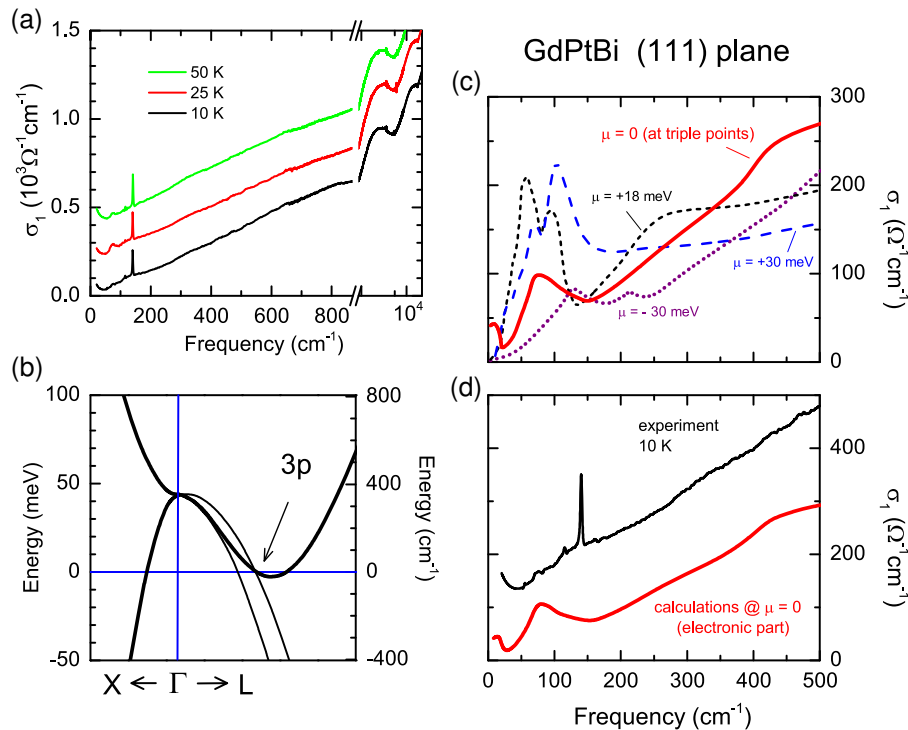


Figure 10. a) Experimental optical conductivity of GdPtBi at three different temperatures (the curves for 25 and 50 K are shifted upward for clarity). b) Band structure of GdPtBi near the triple point (3p). The chemical potential is set to the triple-point position. Doubly degenerate bands are shown as thick lines and nondegenerate bands as thin lines. c) Calculated interband conductivity of GdPtBi for a few different positions of μ as indicated. d) A comparison of the measured (upper curve) and calculated for $\mu = 0$ (bottom curve) optical conductivity of GdPtBi. The sharp phonon mode at around 150 cm^{-1} is not included in the calculated conductivity. The experimental curve is shifted upward by $100 \text{ } \Omega^{-1} \text{ cm}^{-1}$ for clarity. Adapted with permission.^[28] Copyright 2018, American Physical Society.

predominantly, but not exclusively, linear dispersion relations (Figure 10b). We also found that varying the position of the chemical potential within only $\pm 30 \text{ meV}$ drastically changes the overall shape of $\sigma_1^{\text{IB}}(\omega)$, as shown in Figure 10c. Thus, the simple conical dispersion, where μ only affects the frequency position of the Pauli edge, see Equation (3) and (4), is obviously not relevant for GdPtBi.

3.5. Multifold Semimetals

Multifold semimetals—the materials, which possess the characteristic electronic band crossings with degeneracies higher than two^[7,23]—attract currently a lot of attention. This electronic phase may occur in noncentrosymmetric compounds with no mirror planes. A number of multifold semimetals were recently predicted and experimentally confirmed, leading to a realization of “topological chiral crystals.”^[110–116] Among other chirality-related properties, these materials are believed to demonstrate a peculiar nonlinear optical phenomenon—the quantized circular photogalvanic effect (QCPGE).^[117] In this effect, the circularly polarized photons excite the chiral band carriers in such a way that the resultant photocurrent is quantized in units of material-independent fundamental constants. Recently, the observation of QCPGE was reported in RhSi,^[118] an established multifold semimetal.^[111–113] The knowledge of frequency-dependent linear

conductivity in multifold semimetals is also essential, in particular, for a proper interpretation of QCPGE experiments. Herein, we review recent reports on the experimental determination of $\sigma_1(\omega)$ in RhSi^[38,118] and compare the obtained results with the available theoretical calculations.^[58,82] As noticed in Section 2, the optical conductivity of multifold semimetals is supposed to demonstrate a linear-in-frequency $\sigma_1^{\text{IB}}(\omega)$, similarly to 3D Dirac and Weyl semimetals.

Figure 11 shows experimental^[38,118] and calculated^[82] optical conductivities of RhSi. The experimental curves follow each other quite well. The deviations between the curves can be explained by different free-carrier contributions. Despite some discrepancy between the calculations and both experimental curves, the match can be considered as satisfactory (cf. Figure 2 and 3). Both low-energy features of the interband experimental conductivity—the initial (i.e., for the frequencies just above the Drude roll-off) linear increase and the further flattening—are reproduced by theory.

To establish a better connection between the features observed in the most interesting, low-energy, part of the experimental conductivity and the interband optical transitions, in Figure 12 we show $\sigma_1(\omega)$ from the study by Maulana et al.^[38] together with the low-energy band structure of RhSi. The interband contribution to the optical conductivity, $\sigma_1^{\text{IB}}(\omega)$, obtained in the study is also shown. At the lowest frequencies (below $\approx 2500 \text{ cm}^{-1}$), the interband conductivity is entirely caused by transitions in the

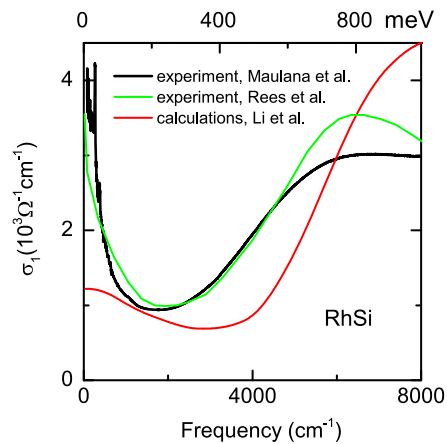


Figure 11. Optical conductivity of the multifold semimetal RhSi. The experimental data are from the study by Maulana et al.^[38] (black line) and from the study by Rees et al.^[118] (green line). The theoretical curve is adapted from the study by Li et al.^[82]

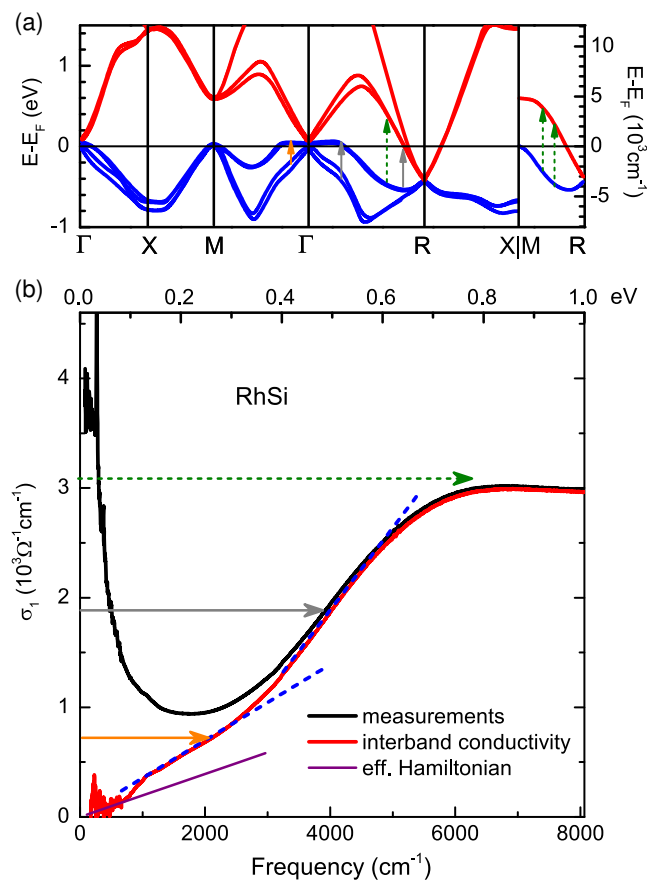


Figure 12. a) Low-energy electronic structure of RhSi and b) its optical conductivity. The optical transitions responsible for the characteristic features in the interband portion of optical conductivity are depicted as vertical arrows in (a). The corresponding frequency scales are indicated by the horizontal arrows of the same color in (b).^[38]

vicinity of the Γ point. No other interband optical transitions are possible (either the direct gap between the bands is too large or the transitions are Pauli blocked). The bands near the Γ point are all roughly linear (two of them are basically flat); thus a linear-in-frequency interband conductivity is expected.^[58] Indeed, $\sigma_1^{\text{IB}}(\omega)$ is proportional to frequency in this range (the orange arrows in both panels of Figure 12). At somewhat higher frequencies ($\approx 3000\text{--}4000\text{ cm}^{-1}$), the flat bands start to disperse downward; thus, the linearity of $\sigma_1^{\text{IB}}(\omega)$ is not expected anymore. However, the interband contributions in the vicinity of R points are allowed at roughly the same energy (see the gray arrows in Figure 12a). These transitions provide a dominating contribution to conductivity, and the linear-in-frequency increase in $\sigma_1^{\text{IB}}(\omega)$ is restored with a larger slope (the gray arrow in Figure 12b). At frequencies above 6000 cm^{-1} , the optical conductivity flattens out, forming a broad flat maximum. It can be attributed to the transitions between the almost (but not exactly) parallel bands along the $M\text{--}R$ line, which are shown as dotted green arrows. The maximum is not sharp because other transitions with comparable energies also contribute at these frequencies; see, e.g., the dotted green arrow between the Γ and R points. Figure 12 also shows the results of effective Hamiltonian calculations^[58] for the contributions near the Γ point. An extrapolation of these calculations (originally performed for frequencies below 320 cm^{-1}) to higher frequencies is shown as a solid purple line. The experimental $\sigma_1^{\text{IB}}(\omega)$ is generally steeper than the results of these calculations. The mismatch can be related to deviations of the bands from linearity even at low energies.^[82,111,112] This can be clarified in more advanced band-structure-based optical conductivity calculations. In any case, the predicted linear run of $\sigma_1^{\text{IB}}(\omega)$ is experimentally confirmed for a multifold semimetal.

3.6. Linear-in-Frequency Conductivity in Other Materials

The fact that 3D Dirac and Weyl semimetals were predicted to demonstrate a quite unusual (linear-in-frequency) optical conductivity, stimulated experimental efforts in finding such $\sigma_1(\omega)$ in different materials and in making proposals based on these observations. For example, Timusk et al.^[65] reported a linear $\sigma_1(\omega)$ in a number of quasicrystals and suggested the presence of 3D Dirac fermions in these materials. To our knowledge, this proposition remains to be confirmed by other experimental methods, as well as by theory. The original forecasts of a Weyl state in pyrochlore iridates^[3] stimulated an optical study of $\text{Eu}_2\text{Ir}_2\text{O}_7$, where linear $\sigma_1(\omega)$ was observed in a limited range at low energies.^[67] Up to now, no firm confirmations of a Weyl state in this or other pyrochlore iridates are reported; they are currently believed to be trivial antiferromagnetic insulators with the important role of electron correlations.^[119–121] Interestingly to note that linear $\sigma_1(\omega)$ in a broad frequency range was observed in BaCoS_2 , another material with strong electron correlations.^[122] This linearity was not attributed to 3D conical bands (which actually do not exist in this compound) but to an effect of electron correlations. These examples, as well as the case of GdPtBi discussed above demonstrate once again that interpretations of linear $\sigma_1(\omega)$ should always be made with care and theory output is essential for such interpretations.

4. Conclusions

When graphene shifted in the focus of condensed matter physics, its constant in frequency conductivity appeared as a peculiarity at first glance. Soon it became clear that this was the tip of an iceberg: materials with interesting band structure and topology are predicted and discovered at a rapid pace since. The Dirac cones in graphene are just a particular case of a class of systems that is not restricted to two dimensions. Different nodal semimetals, possessing conical bands in their bulk, are currently at the center of studies, and conductivity of these materials is directly related to the electronic band dispersion and dimensionality. Albeit ARPES is surely the most proper method to study the band structure and Fermi surface, its severe restriction to the sample surface often causes problems that can be overcome by optical methods, as a genuine bulk sensitive technique. In this brief survey, we considered a representative selection of recent experimental results on optical studies of different nodal semimetals. The presented examples demonstrate the abilities, as well as limitations, of linear optics to reveal the bulk band structure at low energies.

Acknowledgements

The authors thank the Deutsche Forschungsgemeinschaft (DFG) for financial support. Open access funding enabled and organized by Projekt DEAL.

Conflict of Interest

The authors declare no conflict of interest.

Keywords

nodal semimetals, optical conductivity, topological materials

Received: January 14, 2020

Revised: February 27, 2020

Published online: March 24, 2020

-
- [1] S. Murakami, *New J. Phys.* **2007**, *9*, 356.
 [2] A. Kobayashi, S. Katayama, Y. Suzumura, H. Fukuyama, *J. Phys. Soc. Jpn.* **2007**, *76*, 034711.
 [3] X. Wan, A. M. Turner, A. Vishwanath, S. Y. Savrasov, *Phys. Rev. B* **2011**, *83*, 205101.
 [4] A. A. Burkov, L. Balents, *Phys. Rev. Lett.* **2011**, *107*, 127205.
 [5] A. A. Burkov, M. D. Hook, L. Balents, *Phys. Rev. B* **2011**, *84*, 235126.
 [6] J. Park, G. Lee, F. Wolff-Fabris, Y. Y. Koh, M. J. Eom, Y. K. Kim, M. A. Farhan, Y. J. Jo, C. Kim, J. H. Shim, J. S. Kim, *Phys. Rev. Lett.* **2011**, *107*, 126402.
 [7] J. L. Mañes, *Phys. Rev. B* **2012**, *85*, 155118.
 [8] Z. Wang, Y. Sun, X.-Q. Chen, C. Franchini, G. Xu, H. Weng, X. Dai, Z. Fang, *Phys. Rev. B* **2012**, *85*, 195320.
 [9] Z. Wang, H. Weng, Q. Wu, X. Dai, Z. Fang, *Phys. Rev. B* **2013**, *88*, 125427.
 [10] Z. K. Liu, J. Jiang, B. Zhou, Z. J. Wang, Y. Zhang, H. M. Weng, D. Prabhakaran, S.-K. Mo, H. Peng, P. Dudin, T. Kim, M. Hoesch, Z. Fang, X. Dai, Z. X. Shen, D. L. Feng, Z. Hussain, Y. L. Chen, *Nat. Mater.* **2014**, *13*, 677.
 [11] S. Borisenko, Q. Gibson, D. Evtushinsky, V. Zabolotnyy, B. Büchner, R. J. Cava, *Phys. Rev. Lett.* **2014**, *113*, 027603.
 [12] M. Neupane, S.-Y. Xu, R. Sankar, N. Alidoust, G. Bian, C. Liu, I. Belopolski, T.-R. Chang, H.-T. Jeng, H. Lin, A. Bansil, F. Chou, M. Z. Hasan, *Nat. Commun.* **2014**, *5*, 3786.
 [13] O. Vafek, A. Vishwanath, *Annu. Rev. Condens. Matter Phys.* **2014**, *5*, 83.
 [14] B. Q. Lv, H. M. Weng, B. B. Fu, X. P. Wang, H. Miao, J. Ma, P. Richard, X. C. Huang, L. X. Zhao, G. F. Chen, Z. Fang, X. Dai, T. Qian, H. Ding, *Phys. Rev. X* **2015**, *5*, 031013.
 [15] S.-M. Huang, S.-Y. Xu, I. Belopolski, C.-C. Lee, G. Chang, B. Wang, N. Alidoust, G. Bian, M. Neupane, C. Zhang, S. Jia, A. Bansil, H. Lin, M. Z. Hasan, *Nat. Commun.* **2015**, *6*, 7373.
 [16] C. Shekhar, A. K. Nayak, Y. Sun, M. Schmidt, M. Nicklas, I. Leermakers, U. Zeitler, Y. Skourski, J. Wosnitza, Z. Liu, Y. Chen, W. Schnelle, H. Borrmann, Y. Grin, C. Felser, B. Yan, *Nat. Phys.* **2015**, *11*, 645.
 [17] H. Weng, C. Fang, Z. Fang, B. A. Bernevig, X. Dai, *Phys. Rev. X* **2015**, *5*, 011029.
 [18] S.-Y. Xu, I. Belopolski, N. Alidoust, M. Neupane, G. Bian, C. Zhang, R. Sankar, G. Chang, Z. Yuan, C.-C. Lee, S.-M. Huang, H. Zheng, J. Ma, D. S. Sanchez, B. Wang, A. Bansil, F. Chou, P. P. Shibayev, H. Lin, S. Jia, M. Z. Hasan, *Science* **2015**, *349*, 613.
 [19] D.-F. Xu, Y.-P. Du, Z. Wang, Y.-P. Li, X.-H. Niu, Q. Yao, P. Dudin, Z.-A. Xu, X.-G. Wan, D.-L. Feng, *Chin. Phys. Lett.* **2015**, *32*, 107101.
 [20] Z. Wang, Y. Zheng, Z. Shen, Y. Lu, H. Fang, F. Sheng, Y. Zhou, X. Yang, Y. Li, C. Feng, Z.-A. Xu, *Phys. Rev. B* **2016**, *93*, 121112.
 [21] C.-K. Chiu, J. C. Y. Teo, A. P. Schnyder, S. Ryu, *Rev. Mod. Phys.* **2016**, *88*, 035005.
 [22] Z. Zhu, G. W. Winkler, Q. Wu, J. Li, A. A. Soluyanov, *Phys. Rev. X* **2016**, *6*, 031003.
 [23] B. Bradlyn, J. Cano, Z. Wang, M. G. Vergniory, C. Felser, R. J. Cava, B. A. Bernevig, *Science* **2016**, *353*, aaf5037.
 [24] N. P. Armitage, E. J. Mele, A. Vishwanath, *Rev. Mod. Phys.* **2018**, *90*, 015001.
 [25] T. O. Wehling, A. M. Black-Schaffer, A. V. Balatsky, *Adv. Phys.* **2014**, *63*, 1.
 [26] M. B. Schilling, L. M. Schoop, B. V. Lotsch, M. Dressel, A. V. Pronin, *Phys. Rev. Lett.* **2017**, *119*, 187401.
 [27] D. Neubauer, A. Yaresko, W. Li, A. Löhle, R. Hübner, M. B. Schilling, C. Shekhar, C. Felser, M. Dressel, A. V. Pronin, *Phys. Rev. B* **2018**, *98*, 195203.
 [28] F. Hütt, A. Yaresko, M. B. Schilling, C. Shekhar, C. Felser, M. Dressel, A. V. Pronin, *Phys. Rev. Lett.* **2018**, *121*, 176601.
 [29] W. Witczak-Krempa, G. Chen, Y. B. Kim, L. Balents, *Annu. Rev. Condens. Matter Phys.* **2014**, *5*, 57.
 [30] M. Dzero, J. Xia, V. Galitski, P. Coleman, *Annu. Rev. Condens. Matter Phys.* **2016**, *7*, 249.
 [31] D. Liu, K. Ishikawa, R. Takehara, K. Miyagawa, M. Tamura, K. Kanoda, *Phys. Rev. Lett.* **2016**, *116*, 226401.
 [32] J. Fujioka, T. Okawa, A. Yamamoto, Y. Tokura, *Phys. Rev. B* **2017**, *95*, 121102.
 [33] L. Ye, M. Kang, J. Liu, F. von Cube, C. R. Wicker, T. Suzuki, C. Jozwiak, A. Bostwick, E. Rotenberg, D. C. Bell, L. Fu, R. Comin, J. G. Checkelsky, *Nature* **2018**, *555*, 638.
 [34] P. P. Rinkel, P. L. S. Lopes, I. Garate, *Phys. Rev. Lett.* **2017**, *119*, 107401.
 [35] A. Hui, Y. Zhang, E.-A. Kim, *Phys. Rev. B* **2019**, *100*, 085144.
 [36] M. Corasaniti, R. Yang, A. Pal, M. Chinotti, L. Degiorgi, A. Wang, C. Petrovic, *Phys. Rev. B* **2019**, *100*, 041107.
 [37] B. Xu, Y. M. Dai, L. X. Zhao, K. Wang, R. Yang, W. Zhang, J. Y. Liu, H. Xiao, G. F. Chen, S. A. Trugman, J.-X. Zhu, A. J. Taylor, D. A. Yarotski, R. P. Prasankumar, X. G. Qiu, *Nat. Commun.* **2017**, *8*, 14933.

- [38] L. Z. Maulana, K. Manna, E. Uykur, C. Felser, M. Dressel, A. V. Pronin, arXiv:1911.11538, **2019**.
- [39] P. E. C. Ashby, J. P. Carbotte, *Phys. Rev. B* **2014**, *89*, 245121.
- [40] J. P. Carbotte, *Phys. Rev. B* **2016**, *94*, 165111.
- [41] C. J. Tabert, J. P. Carbotte, E. J. Nicol, *Phys. Rev. B* **2016**, *93*, 085426.
- [42] C. J. Tabert, J. P. Carbotte, *Phys. Rev. B* **2016**, *93*, 085442.
- [43] J. P. Carbotte, *J. Phys.: Condens. Matter* **2017**, *29*, 045301.
- [44] S. P. Mukherjee, J. P. Carbotte, *Phys. Rev. B* **2017**, *95*, 214203.
- [45] S. P. Mukherjee, J. P. Carbotte, *J. Phys.: Condens. Matter* **2017**, *29*, 425301.
- [46] S. P. Mukherjee, J. P. Carbotte, *Phys. Rev. B* **2018**, *97*, 045150.
- [47] J. P. Carbotte, K. R. Bryenton, E. J. Nicol, *Phys. Rev. B* **2019**, *99*, 115406.
- [48] J. P. Carbotte, E. J. Nicol, *Phys. Rev. B* **2019**, *100*, 035441.
- [49] P. Hosur, S. A. Parameswaran, A. Vishwanath, *Phys. Rev. Lett.* **2012**, *108*, 046602.
- [50] A. Bácsí, A. Virosztek, *Phys. Rev. B* **2013**, *87*, 125425.
- [51] M. Dressel, G. Grüner, *Electrodynamics of Solids*, Cambridge University Press, Cambridge **2002**.
- [52] A. A. Soluyanov, D. Gresch, Z. Wang, Q. Wu, M. Troyer, X. Dai, B. A. Bernevig, *Nature* **2015**, *527*, 495.
- [53] Y. Xu, F. Zhang, C. Zhang, *Phys. Rev. Lett.* **2015**, *115*, 265304.
- [54] G. Xu, H. Weng, Z. Wang, X. Dai, Z. Fang, *Phys. Rev. Lett.* **2011**, *107*, 186806.
- [55] C. Fang, M. J. Gilbert, X. Dai, B. A. Bernevig, *Phys. Rev. Lett.* **2012**, *108*, 266802.
- [56] S.-M. Huang, S.-Y. Xu, I. Belopolski, C.-C. Lee, G. Chang, T.-R. Chang, B. Wang, N. Alidoust, G. Bian, M. Neupane, D. Sanchez, H. Zheng, H.-T. Jeng, A. Bansil, T. Neupert, H. Lin, M. Z. Hasan, *Proc. Natl. Acad. Sci. USA* **2016**, *113*, 1180.
- [57] B. Singh, G. Chang, T.-R. Chang, S.-M. Huang, C. Su, M.-C. Lin, H. Lin, A. Bansil, *Sci. Rep.* **2018**, *8*, 10540.
- [58] M.-A. Sánchez-Martínez, F. de Juan, A. G. Grushin, *Phys. Rev. B* **2019**, *99*, 155145.
- [59] S. Ahn, E. J. Mele, H. Min, *Phys. Rev. B* **2017**, *95*, 161112.
- [60] T. Ando, Y. Zheng, H. Suzuura, *J. Phys. Soc. Jpn.* **2002**, *71*, 1318.
- [61] K. F. Mak, M. Y. Sfeir, Y. Wu, C. H. Lui, J. A. Misewich, T. F. Heinz, *Phys. Rev. Lett.* **2008**, *101*, 196405.
- [62] A. B. Kuzmenko, E. van Heumen, F. Carbone, D. van der Marel, *Phys. Rev. Lett.* **2008**, *100*, 117401.
- [63] S. Ahn, E. J. Mele, H. Min, *Phys. Rev. Lett.* **2017**, *119*, 147402.
- [64] K. Ueda, Y. Fujioka, Y. Takahashi, T. Suzuki, S. Ishiwata, Y. Taguchi, Y. Tokura, *Phys. Rev. Lett.* **2012**, *109*, 136402.
- [65] T. Timusk, J. P. Carbotte, C. C. Homes, D. N. Basov, S. G. Sharapov, *Phys. Rev. B* **2013**, *87*, 235121.
- [66] R. Y. Chen, S. J. Zhang, J. A. Schneeloch, C. Zhang, Q. Li, G. D. Gu, N. L. Wang, *Phys. Rev. B* **2015**, *92*, 075107.
- [67] A. B. Sushkov, J. B. Hofmann, G. S. Jenkins, J. Ishikawa, N. Nakatsuji, S. Das Sarma, H. D. Drew, *Phys. Rev. B* **2015**, *92*, 241108.
- [68] B. Xu, Y. M. Dai, L. X. Zhao, K. Wang, R. Yang, W. Zhang, J. Y. Liu, H. Xiao, G. F. Chen, A. J. Taylor, D. A. Yarotski, R. P. Prasankumar, X. G. Qiu, *Phys. Rev. B* **2016**, *93*, 121110.
- [69] M. Chinotti, A. Pal, W. J. Ren, C. Petrovic, L. Degiorgi, *Phys. Rev. B* **2016**, *94*, 245101.
- [70] D. Neubauer, J. P. Carbotte, A. A. Nateprov, A. Löhle, M. Dressel, A. V. Pronin, *Phys. Rev. B* **2016**, *93*, 121202.
- [71] M. B. Schilling, A. Löhle, D. Neubauer, C. Shekhar, C. Felser, M. Dressel, A. V. Pronin, *Phys. Rev. B* **2017**, *95*, 155201.
- [72] Z. Qiu, C. Le, Y. Dai, B. Xu, J. B. He, R. Yang, G. Chen, J. Hu, X. Qiu, *Phys. Rev. B* **2018**, *98*, 115151.
- [73] R. Kemmler, R. Hübner, A. Löhle, D. Neubauer, I. Voloshenko, L. M. Schoop, M. Dressel, A. V. Pronin, *J. Phys.: Condens. Matter* **2018**, *30*, 485403.
- [74] B. Xu, L. X. Zhao, P. Marsik, E. Sheveleva, F. Lyzwa, Y. M. Dai, G. F. Chen, X. G. Qiu, C. Bernhard, *Phys. Rev. Lett.* **2018**, *121*, 187401.
- [75] E. Martino, I. Crassee, G. Eguchi, D. Santos-Cottin, R. D. Zhong, G. D. Gu, H. Berger, Z. Rukelj, M. Orlita, C. C. Homes, A. Akrap, *Phys. Rev. Lett.* **2019**, *122*, 217402.
- [76] Z. Qiu, C. Le, Z. Liao, B. Xu, R. Yang, J. Hu, Y. Dai, X. Qiu, *Phys. Rev. B* **2019**, *100*, 125136.
- [77] Z.-Y. Qiu, Z.-Y. Liao, X.-G. Qiu, *Chin. Phys. B* **2019**, *28*, 047801.
- [78] D. Grassano, F. Bechstedt, O. Pulci, *J. Appl. Phys.* **2018**, *124*, 205110.
- [79] D. Grassano, O. Pulci, A. M. Conte, F. Bechstedt, *Sci. Rep.* **2018**, *8*, 3534.
- [80] T. Habe, M. Koshino, *Phys. Rev. B* **2018**, *98*, 125201.
- [81] T. Habe, *Phys. Rev. B* **2019**, *100*, 245131.
- [82] Z. Li, T. Iitaka, H. Zeng, H. Su, *Phys. Rev. B* **2019**, *100*, 155201.
- [83] D. Chaudhuri, B. Cheng, A. Yaresko, Q. D. Gibson, R. J. Cava, N. P. Armitage, *Phys. Rev. B* **2017**, *96*, 075151.
- [84] J. Ebad-Allah, J. F. Afonso, M. Krottenmüller, J. Hu, Y. L. Zhu, Z. Q. Mao, J. Kuneš, C. A. Kuntscher, *Phys. Rev. B* **2019**, *99*, 125154.
- [85] Y. Shao, Z. Sun, Y. Wang, C. Xu, R. Sankar, A. J. Breindel, C. Cao, M. M. Fogler, A. J. Millis, F. Chou, Z. Li, T. Timusk, M. B. Maple, D. N. Basov, *Proc. Natl. Acad. Sci. USA* **2019**, *116*, 1168.
- [86] L. M. Schoop, M. N. Ali, C. Straßer, A. Topp, A. Varykhalov, D. Marchenko, V. Duppel, S. S. P. Parkin, B. V. Lotsch, C. R. Ast, *Nat. Comm.* **2016**, *7*, 11696.
- [87] M. Neupane, I. Belopolski, M. M. Hosen, D. S. Sanchez, R. Sankar, M. Szwalska, S.-Y. Xu, K. Dimitri, N. Dhakal, P. Maldonado, P. M. Oppeneer, D. Kaczorowski, F. Chou, M. Z. Hasan, T. Durakiewicz, *Phys. Rev. B* **2016**, *93*, 201104.
- [88] J. Ebad-Allah, M. Krottenmüller, J. Hu, Y. L. Zhu, Z. Q. Mao, C. A. Kuntscher, *Phys. Rev. B* **2019**, *99*, 245133.
- [89] E. Uykur, L. Z. Maulana, L. M. Schoop, B. V. Lotsch, M. Dressel, A. V. Pronin, *Phys. Rev. Res.* **2019**, *1*, 032015.
- [90] L. X. Yang, Z. K. Liu, Y. Sun, H. Peng, H. F. Yang, T. Zhang, B. Zhou, Y. Zhang, Y. F. Guo, M. Rahn, D. Prabhakaran, Z. Hussain, S.-K. Mo, C. Felser, B. Yan, Y. L. Chen, *Nat. Phys.* **2015**, *11*, 728.
- [91] C.-C. Lee, S.-Y. Xu, S.-M. Huang, D. S. Sanchez, I. Belopolski, G. Chang, G. Bian, N. Alidoust, H. Zheng, M. Neupane, B. Wang, A. Bansil, M. Z. Hasan, H. Lin, *Phys. Rev. B* **2015**, *92*, 235104.
- [92] S.-i. Kimura, H. Yokoyama, H. Watanabe, J. Sichelschmidt, V. Süß, M. Schmidt, C. Felser, *Phys. Rev. B* **2017**, *96*, 075119.
- [93] S. Polatkan, M. O. Goerbig, J. Wyzula, R. Kemmler, L. Z. Maulana, B. A. Piot, I. Crassee, A. Akrap, C. Shekhar, C. Felser, M. Dressel, A. V. Pronin, M. Orlita, arXiv:1912.07327, **2019**.
- [94] A. L. Levy, A. B. Sushkov, F. Liu, B. Shen, N. Ni, H. D. Drew, G. S. Jenkins, *Phys. Rev. B* **2020**, *101*, 125102.
- [95] S. Jeon, B. B. Zhou, A. Gyenis, B. E. Feldman, I. Kimchi, A. C. Potter, Q. D. Gibson, R. J. Cava, A. Vishwanath, A. Yazdani, *Nat. Mater.* **2014**, *13*, 851.
- [96] I. Crassee, E. Martino, C. C. Homes, O. Caha, J. Novák, P. Tückmantel, M. Hakl, A. Nateprov, E. Arushanov, Q. D. Gibson, R. J. Cava, S. M. Koohpayeh, K. E. Arpino, T. M. McQueen, M. Orlita, A. Akrap, *Phys. Rev. B* **2018**, *97*, 125204.
- [97] G. S. Jenkins, C. Lane, B. Barbiellini, A. B. Sushkov, R. L. Carey, F. Liu, J. W. Krizan, S. K. Kushwaha, Q. Gibson, T.-R. Chang, H.-T. Jeng, H. Lin, R. J. Cava, A. A. Bansil, H. D. Drew, *Phys. Rev. B* **2016**, *94*, 085121.
- [98] A. Akrap, M. Hakl, S. Tchoumakov, I. Crassee, J. Kuba, M. O. Goerbig, C. C. Homes, O. Caha, J. Novák, F. Teppe, W. Desrat, S. Koohpayeh, L. Wu, N. P. Armitage, A. Nateprov, E. Arushanov, Q. D. Gibson, R. J. Cava, D. van der Marel, B. A. Piot, C. Faugeras, G. Martinez, M. Potemski, M. Orlita, *Phys. Rev. Lett.* **2016**, *117*, 136401.

- [99] E. Uykur, R. Sankar, D. Schmitz, C. A. Kuntscher, *Phys. Rev. B* **2018**, 97, 195134.
- [100] I. Crassee, R. Sankar, W.-L. Lee, A. Akrap, M. Orlita, *Phys. Rev. Mater.* **2018**, 2, 120302.
- [101] E. O. Kane, *J. Phys. Chem. Solids* **1957**, 1, 249.
- [102] J. Bodnar, *Physics of Narrow Gap Semiconductors: Proceedings of the III International Conference*, Warszawa, September 12–15, 1977 (Eds: J. Rautuszkiewicz, M. Górska, E. Kaczmarek), Elsevier, Amsterdam **1978**.
- [103] J. Bodnar, arXiv:1709.05845, **2017**.
- [104] R. Beyer, A. Dengl, T. Peterseim, S. Wackerow, T. Ivek, A. V. Pronin, D. Schweitzer, M. Dressel, *Phys. Rev. B* **2016**, 93, 195116.
- [105] A. J. Frenzel, C. C. Homes, Q. D. Gibson, Y. M. Shao, K. W. Post, A. Charnukha, R. J. Cava, D. N. Basov, *Phys. Rev. B* **2017**, 95, 245140.
- [106] S.-i. Kimura, Y. Nakajima, Z. Mita, R. Jha, R. Higashinaka, T. D. Matsuda, Y. Aoki, *Phys. Rev. B* **2019**, 99, 195203.
- [107] S. Chadov, X. Qi, J. Kübler, G. H. Fecher, C. Felser, S. C. Zhang, *Nat. Mater.* **2010**, 9, 541.
- [108] H. Lin, L. A. Wray, Y. Xia, S. Xu, S. Jia, R. J. Cava, A. Bansil, M. Z. Hasan, *Nat. Mater.* **2010**, 9, 546.
- [109] P. C. Canfield, J. D. Thompson, W. P. Beyermann, A. Lacerda, M. F. Hundley, E. Peterson, Z. Fisk, *J. Appl. Phys.* **2016**, 70, 1991.
- [110] G. Chang, B. J. Wieder, F. Schindler, D. S. Sanchez, I. Belopolski, S.-M. Huang, B. Singh, D. Wu, T.-R. Chang, T. Neupert, S.-Y. Xu, H. Lin, M. Z. Hasan, *Nat. Mater.* **2018**, 17, 978.
- [111] G. Chang, S.-Y. Xu, B. J. Wieder, D. S. Sanchez, S.-M. Huang, I. Belopolski, T.-R. Chang, S. Zhang, A. Bansil, H. Lin, M. Z. Hasan, *Phys. Rev. Lett.* **2017**, 119, 206401.
- [112] P. Tang, Q. Zhou, S.-C. Zhang, *Phys. Rev. Lett.* **2017**, 119, 206402.
- [113] D. S. Sanchez, I. Belopolski, T. A. Cochran, X. Xu, J.-X. Yin, G. Chang, W. Xie, K. Manna, V. Süß, C.-Y. Huang, N. Alidoust, D. Multer, S. S. Zhang, N. Shumiya, X. Wang, G.-Q. Wang, T.-R. Chang, C. Felser, S.-Y. Xu, S. Jia, H. Lin, M. Z. Hasan, *Nature* **2019**, 567, 500.
- [114] Z. Rao, H. Li, T. Zhang, S. Tian, C. Li, B. Fu, C. Tang, L. Wang, Z. Li, W. Fan, J. Li, Y. Huang, Z. Liu, Y. Long, C. Fang, H. Weng, Y. Shi, H. Lei, Y. Sun, T. Qian, H. Ding, *Nature* **2019**, 567, 496.
- [115] N. B. M. Schröter, D. Pei, M. G. Vergniory, Y. Sun, K. Manna, F. de Juan, J. A. Krieger, V. Süss, M. Schmidt, P. Dudin, B. Bradlyn, T. K. Kim, T. Schmitt, C. Cacho, C. Felser, V. N. Strocov, Y. Y. Chen, *Nat. Phys.* **2019**, 15, 759.
- [116] D. Takane, Z. Wang, S. Souma, K. Nakayama, T. Nakamura, H. Oinuma, Y. Nakata, H. Iwasawa, C. Cacho, T. Kim, K. Horiba, H. Kumigashira, T. Takahashi, Y. Ando, T. Sato, *Phys. Rev. Lett.* **2019**, 122, 076402.
- [117] F. de Juan, A. G. Grushin, T. Morimoto, J. E. Moore, *Nat. Commun.* **2017**, 8, 15995.
- [118] D. Rees, K. Manna, B. Lu, T. Morimoto, H. Borrmann, C. Felser, J. E. Moore, D. H. Torchinsky, J. Orenstein, arXiv:1902.03230, **2019**.
- [119] M. Nakayama, T. Kondo, Z. Tian, J. J. Ishikawa, M. Halim, C. Bareille, W. Malaeb, K. Kuroda, T. Tomita, S. Ideta, K. Tanaka, M. Matsunami, S. Kimura, N. Inami, K. Ono, H. Kumigashira, L. Balents, S. Nakatsuji, S. Shin, *Phys. Rev. Lett.* **2016**, 117, 056403.
- [120] R. Wang, A. Go, A. J. Millis, *Phys. Rev. B* **2017**, 95, 045133.
- [121] Y. Wang, H. Weng, L. Fu, X. Dai, *Phys. Rev. Lett.* **2017**, 119, 187203.
- [122] D. Santos-Cottin, Y. Klein, P. Werner, T. Miyake, L. de' Medici, A. Gauzzi, R. P. S. M. Lobo, M. Casula, *Phys. Rev. Materials* **2018**, 2, 105001.